Article:
Rooke, J., Li, X. and Dwyer-Joyce, R.S. (2022) Applying the Hilbert Envelope method to refine the ultrasonic technique for piston ring oil film thickness measurements in a marine diesel engine. SAE International Journal of Engines, 16 (2). 03-16-02-0011. ISSN: 1946-3936

https://doi.org/10.4271/03-16-02-0011

Applying the Hilbert Envelope method to refine the ultrasonic technique for piston ring oil film thickness measurements in a marine diesel engine

J. Rooke[1], X. Li[2], R. S. Dwyer-Joyce[1]

1 – Leonardo Centre for Tribology, University of Sheffield, Sheffield, UK

2 – Peak to Peak Measurement Solutions Ltd., Broad Lane, Sheffield, S3 7HQ

Corresponding authors:

J. Rooke: jack.o.rooke@gmail.com

R. S. Dwyer-Joyce: r.dwyer-joyce@sheffield.ac.uk

Abstract

The greatest frictional contributor in an internal combustion engine is the contact between the piston/ring pack and cylinder liner. Therefore, an improved lubrication regime has the potential to raise engine efficiency whilst lowering emissions, aiding to meeting environmental regulations. Previous ultrasonic measurements of the oil film thickness between piston rings and the cylinder liner in a marine engine have been subject to several unexpected trends. This article refines the measurement to identify and remove these factors, the trends were found to have arisen due to the detection of ultrasonic reflections from the piston ring outside of the expected alignment zone. The extent of these undesired reflections is thought to be due to the liner thickness providing a relatively large distance for spreading of the ultrasonic wavefront. The hitherto used Frequency Index method (index the fast Fourier transform at the transducer central frequency) has been compared to the Hilbert Envelope method (index at the peak of the Hilbert envelope) to define the reflection coefficient. The Hilbert Envelope method was found to minimize the impact from reflections outside of the alignment zone leading to more consistent and expected trends in the reflection coefficient. The oil film thickness determined using the Hilbert Envelope method was typically 20% greater than that of the Frequency Index method, indicating the previous method provided an under estimation of the film thickness. Using the Hilbert Envelope method, the oil film thickness for the first piston ring at the top dead center was found to vary from 8.9 μm at full load to 10.4 μm at 25% loading.

Keywords

Diesel marine engine, Ultrasound, Oil film thickness, Piston ring

1 Introduction

The international shipping sector contributes 2.2% of anthropogenic CO_2 emissions [1], with a significant portion of this from marine diesel engines. To reduce the emissions from this sector the International Maritime Organization has set greenhouse gas emission reduction targets, of at least 40% by 2030 relative to 2008 levels. To meet these targets novel technologies are required. Typically, in an engine, 9-20% of the energy in the fuel is wasted due to parasitic losses [2]–[4] with a quarter of those losses from the piston ring pack [5]. In addition, in some engines 40-60% of particulate emissions arise due to lubricant throw off into the combustion chamber [6], [7]. Therefore, improved engine efficiency and an emission

reduction can be achieved via an improved lubrication regime between the piston ring and cylinder liner. Refining the interaction between the piston/ring pack and cylinder liner in combination with using alternative fuels such as liquefied natural gas, methanol or bio-methanol [8] and refining the combustion cycle [9] provides a viable route to meet environmental regulations.

This article follows the work given in [10] on an RTX-6 Winterthur Gas & Diesel test engine in which a series of ultrasonic sensors were instrumented close to the top dead center (TDC) of the piston and three lubricant injection configurations were evaluated. The ultrasonic sensors provided a methodology to show a novel lubricant injector design led to thicker oil films between the piston ring and liner by a reduction in lubricant lost to the exhaust manifold. This was achieved by reducing the rate of lubricant atomization. This paper extends the previous analysis with an in-depth study of the reflected ultrasonic waves to refine the data processing technique and remove undesired reflections in the data enabling a more accurate measure of the true oil film.

2 Background

The need for in-situ piston ring oil film thickness (OFT) measurements in internal combustion engines has led to a series of techniques being developed. The majority of approaches focus on: electromagnetism, light, or sound [11] and often study the piston rings at, or near their TDC positions due to the reduced piston velocity (and zero velocity at the TDC). This leads to an increased likelihood of boundary lubrication and therefore a greater amount of friction, further to this, a significant portion of lubricant throw off occurs in this region.

The predominant electrical technique uses the capacitance formed between two parallel electrodes of differing potentials: the piston ring and a capacitance probe mounted flush on the internal surface of the liner. Capacitance probes have been used in a range of works and have recorded minimum oil films ranging from 0.2-9 μm [12]–[18]. The method is hindered by excessively thin films (< 1 μm) as metal-metal contact may short the circuit. Furthermore, the dielectric constant is dependent on the nature of the oil film between the piston ring and liner, therefore any cavitation or starvation leads to an overestimation of the true oil film. Due to this, capacitance is often more appropriate for minimum OFT measurements.

Optical techniques such a laser-induced fluorescence (LIF) involve replacing a section of the cylinder liner with a transparent material such that a laser may be shone onto the oil film. Photons in the oil excite and move to a higher energy state, on returning to their original state photos of a different wavelength are emitted and can be correlated to the OFT. The technique has been applied to numerous engines and measured films from 0.4-18 μm [19]–[24] and does not require a full lubricating film between the piston ring and transparent window like the capacitance technique. This enables LIF to be capable of measurements such as residual oil levels on the cylinder liner.

Both LIF and capacitance are invasive techniques and require replacing a portion of the liner internal surface with either a sensor or transparent material. This is also the case in several other techniques; inductance [25], [26], resistance [27], and strain gauge [28]. Alternatively, ultrasound is non-invasive, as the sensor is bonded to the external surface of the cylinder liner. This technique, therefore, requires less modification to the engine and has the potential to give a more representative measure of the oil film as neither of the bounding surfaces of

the oil film is altered. The ultrasonic method uses piezoelectric transducers to pulse and receive ultrasonic waves that have a partial reflection, partial transmittance from each surface which can be correlated to the OFT. This method has been applied to a series of automotive engines [11], [29]–[34] producing minimum OFT measurements of 2-21 μm. The technique has also been applied to a marine diesel engine; in [35] a sensor was mounted behind a piston ring for measurements over the whole piston stroke. Whilst in the previous work on the RTX-6 engine in [10], the minimum OFT for the first ring at the TDC ranged from 5-10 μm at full engine loading. The piezoelectric sensors produce an average measurement over the complete surface of the sensor, therefore, the size of the sensor relative to the piston ring width has a significant impact on the results. For an improved spatial resolution, the sensor width should be less than the width of the piston rings.

The ultrasonic technique is based upon the principle that an ultrasonic wave propagating through a media has a partial reflection/partial transmittance at each discontinuity. The proportion of each depends upon the contact formed between the two media. The proportion reflected relative to the incident is termed the reflection coefficient, *R*. This term is solely dependent upon the acoustic impedance mismatch between the two media, see Equation 1. In which *z*, is the acoustic impedance of each media and is the product of the speed of sound and density.

$$R = \frac{z_2 - z_1}{z_2 + z_1} \quad (1)$$

Surfaces that are separated by a thin oil film (< 20 μm) can be modeled using the Quasi-Static Spring Model [36]. The model assumes the two media are connected by a series of springs within their elastic limit, and thus the stiffness of the spring affects the magnitude of the reflected portion of the ultrasonic wave. This model refines the reflection coefficient definition seen in Equation 1 to Equation 2 in which, *K*, is the interfacial stiffness, and ω is the angular frequency.

$$R = \frac{z_2 - z_1 + \frac{i\omega z_1 z_2}{K}}{z_2 + z_1 + \frac{i\omega z_1 z_2}{K}} \quad (2)$$

Equation 2 can be rearranged to define the thickness of the lubricating film as the stiffness of the lubricating film is dependent upon the lubricant layer thickness, *h*, and the liquid bulk modulus, *B*:

$$K = \frac{B}{h} \quad (3)$$

The bulk modulus of the fluid can be rewritten as the product of the fluid density, ρ, and speed of sound, *c*:

$$K = \frac{\rho c^2}{h} \quad (4)$$

Combination of the refined reflection coefficient in Equation 2 and the interfacial stiffness definition in Equation 4 can be rearranged for an equation of the OFT between a piston ring and liner [37]:

$$h = \frac{\rho c^2}{\omega z_1 z_2} \sqrt{\frac{|R^2|(z_2 + z_1)^2 - (z_2 - z_1)^2}{1 - R^2}} \quad (5)$$

3 Test engine

The fired engine testing was performed on a two-stroke Winterthur Gas & Diesel RTX-6 engine, see *Figure 1*. The major engine parameters are shown in *Table 1*.

Figure 1 RTX-6 test engine reproduced from [10]. © SAE International

Table 1 Engine parameters.

Engine Parameter	Value	Unit
Max power	6470	kW
No. of cylinders	4	-
Cylinder bore	500	mm
Piston stroke	2250	mm

The OFT calculated from the ultrasonic technique is highly dependent on the speed of sound and density of the oil (see Equation 5). To ensure representative results, the speed of sound and density variation with temperature, T, and pressure, p, was measured at a range of values and results were curved fit. This defined Equation 6 and 7 for the speed of sound and density respectively.

$$c = 0.0039T^2 - 3.39T + 4.13p + 1555.2 \quad (6)$$

$$\rho = 162.85 + \frac{888}{1 + 0.007(T - 20)} - \frac{5.88x10^4}{p + 3.61x10^2} \quad (7)$$

3.1 Ultrasonic instrumentation

Five 1 MHz longitudinal ultrasonic sensors were bonded onto the external surface of the RTX-6 liner, see *Figure 2*. This article follows results from two of these sensors, the 'Top

Ring sensor' aligned with the first piston ring at the TDC. As well as the 'Control sensor', an ultrasonic sensor that was intentionally instrumented above all piston rings at their TDC positions to study the effect of cylinder liner distortion, see *Figure 3* for a visualization of their respective locations. The Top Ring sensor and the other longitudinal sensors are also covered in [10].

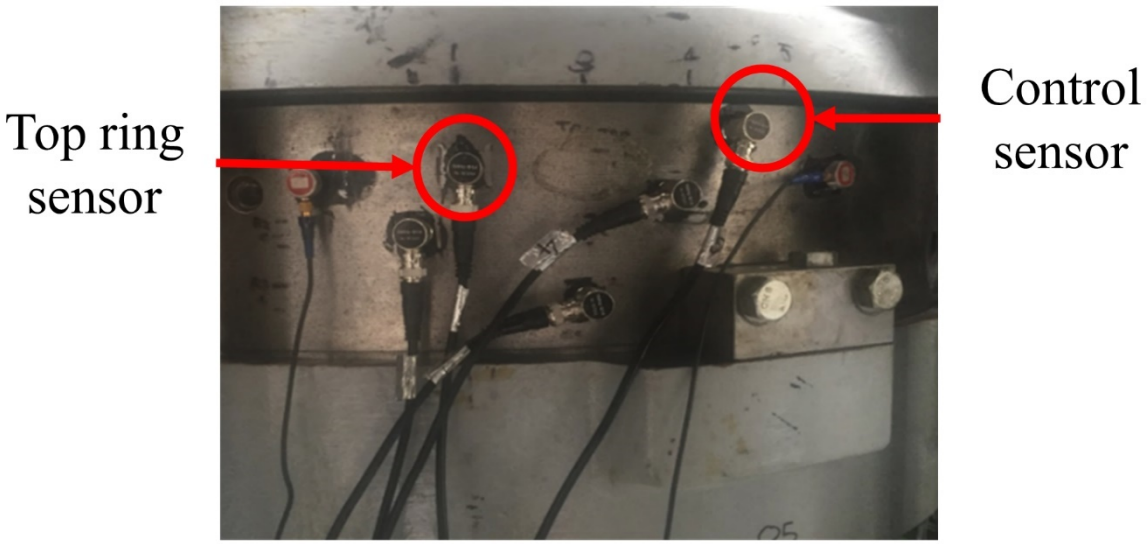

Figure 2 Instrumented ultrasonic sensors.

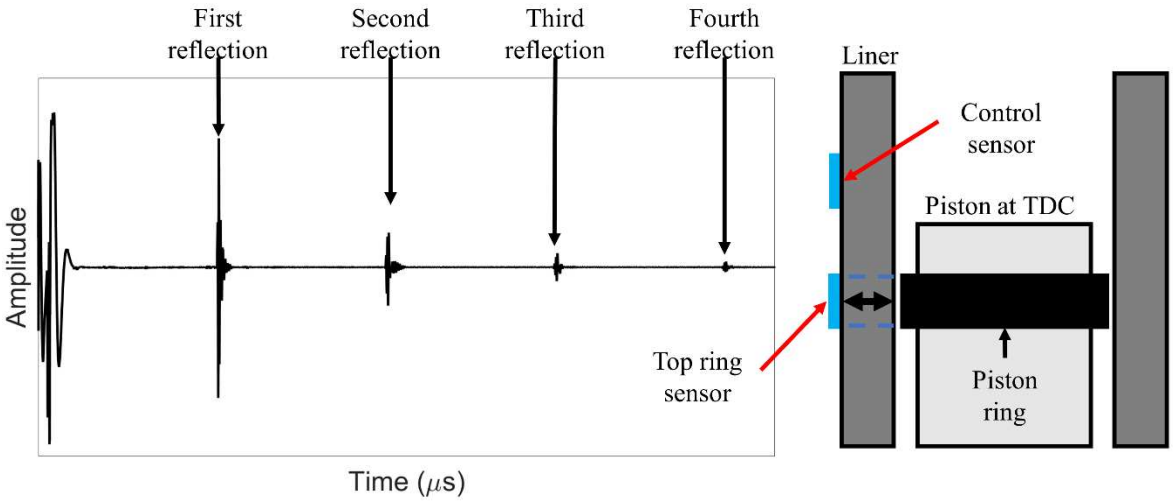

Figure 3 An A-scan showing four ultrasonic reflections from the internal surface of an engine liner and ultrasonic sensor locations.

Each piezoelectric sensor had a 14 mm active element diameter which was less than the width of each of the piston rings. The sensors were coupled to the liner external surface with an industrial adhesive and cured overnight at room temperature. Access to the liner led the sensors to be bonded on the neutral side of the liner, however, and critically, no modifications were made to the engine to enable this study.

The ultrasonic signals were recorded and managed using an ultrasonic pulser receiver (UPR), see *Figure 4*. The unit contains a card that can generate short voltage pulses which the piezoelectric sensors covert to a mechanical displacement instigating a pressure wave in the liner. The wave is reflected from the liner internal surface/piston ring and is received by the sensor. The reflected wave is converted back into a voltage which is digitized in the UPR and a LabView program is used to visualize and record the signal. The captured signal is termed an A-scan, see *Figure 3* which shows 4 successive reflections of a typical ultrasonic wave.

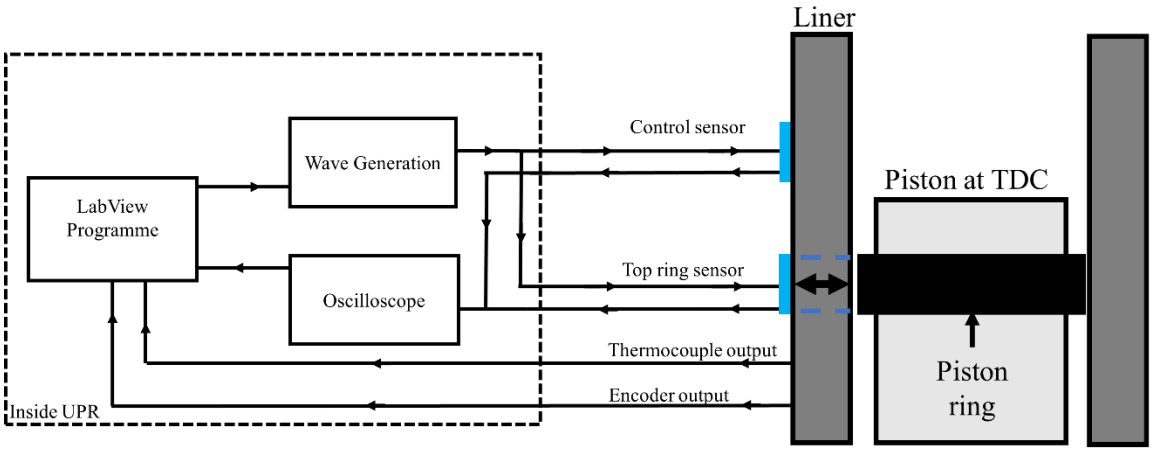

Figure 4 Selection of ultrasonic testing instrumentation.

A data recording lasted 5 seconds, leading to multiple engine cycles being recorded in each capture. The ultrasonic signals were pulsed a 1.05 kHz for each sensor, significantly higher than the speed of the engine, peaking at 105.5 rpm. The ultrasonic data was aligned to piston crank angle (CA) using a shaft encoder which produced a tick for every piston TDC and degree rotation of the engine.

3.2 Test conditions

The marine engine was run at steady-state for three different loading levels (100%, 50%, and 25%), data was captured both inside and outside of the steady-state operation for each loading level. A summary of the loading sequence is shown in *Figure 5*. Each loading step is associated with a different engine speed; 100% - 105.5 rpm, 50% - 83.6 rpm, 25% - 66.2 rpm.

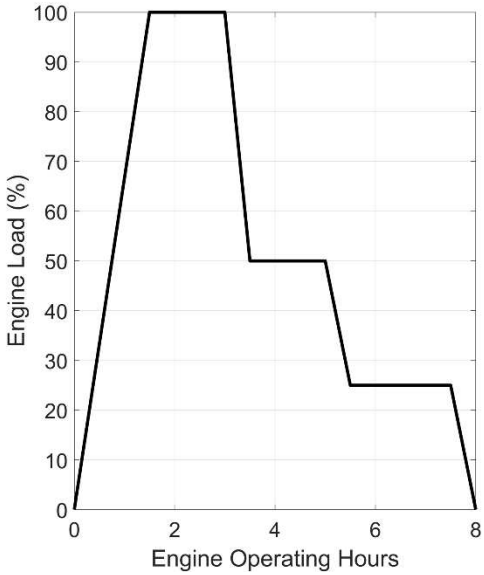

Figure 5 Engine loading variation for each engine configuration, reproduced from [10]. © SAE International

3.3 Signal processing

The raw data was captured as a series of isolated reflections see *Figure 6(a)-(b)*. The common technique to convert these reflections into oil film thickness measurements is shown in the preceding steps of *Figure 6*. The steps can be summarized as; isolate each reflection, convert the signal into the frequency domain; normalize the fast Fourier transform (FFT) relative to the reference FFT (reflection coefficient), and input into the Spring Model (Equation 5). The reference FFT was defined from the mean reflection when the piston ring was significantly far from the sensor, see the red highlighted region in *Figure 6(a)*. The oil film thickness calculation can be refined by using temperature and pressure measurements from the liner internal surface to define the oil speed of sound and density under the conditions experienced above the sensor, see Equations 6 and 7.

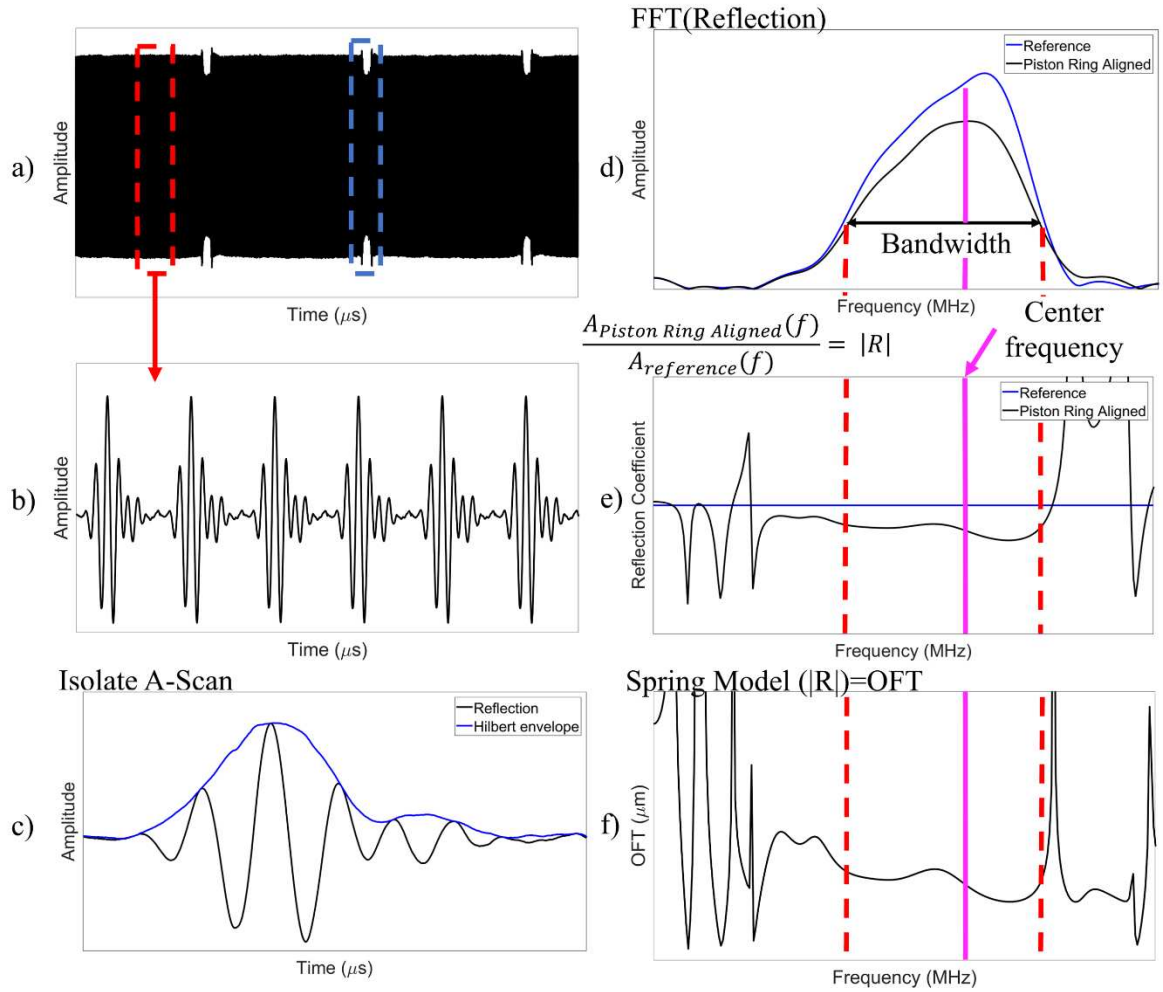

Figure 6 (a) Raw captured data, the highlighted blue region shows the change in reflection amplitude that corresponds to the piston passing the Top Ring sensor. (b) Zoomed-in version of (a) showing the data consists of a series of reflections. (c) Isolated individual reflection, including the Hilbert envelope (d) Reference FFT vs Aligned piston ring FFT. (e) Reflection coefficient variation over the frequency domain. The dashed line corresponds to full reflection (R = 1). (f) OFT over the frequency domain. Figure modified from [10]. © SAE International

The process in *Figure 6* defines the OFT over the whole bandwidth of the ultrasonic sensor, however, the frequency used for OFT measurements is that of the central frequency for the transducer, in the case of this work at 1 MHz. This methodology defines the 'Frequency Index' method that is commonly used for piston ring OFT measurements. Applying this process to the data from the Top Ring sensor produces the reflection coefficient as shown in *Figure 7* for 100% loading, steady-state operation. The region in which the piston ring is aligned over the sensor is highlighted with the blue box.

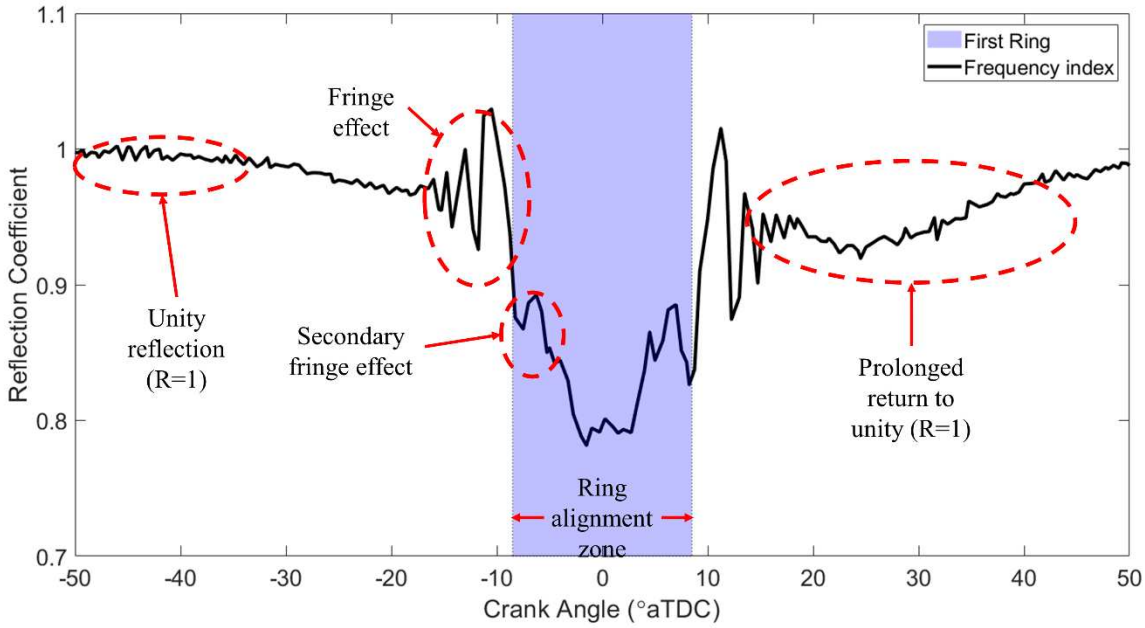

Figure 7 Reflection coefficient for the Top Ring sensor at 100% loading using the Frequency Index method.

When the piston ring was not aligned with the sensor i.e., a solid-gaseous boundary, a complete ultrasonic reflection is seen, leading to R=1, in *Figure 7* from -50° to -40° CA. Whilst when a piston ring moves over the sensor, a reduction in the reflection coefficient is seen, as a greater portion of the wave is transmitted into the ring. In this test case, the minimum reflection coefficient is around 0.75 and can be used to define the minimum OFT (Equation 5). Further to the main features, there are several secondary features (as labeled in *Figure 7*) that are similar to those in other ultrasonic works [10], [38], [39]:

- There is a fringe effect before and after the piston ring, resulting in a series of peaks.
- Inside the alignment region, there is a secondary fringe on either side of the TDC.
- Post ring there is an extended prolonged return to unity reflection coefficient.

The presence of these factors in and around the alignment region of the piston ring, therefore, has the potential to be impacting the calculated oil films, that have been previously defined using the FFT Frequency Index method in [10].

4 B-scans

The potential cause of the secondary features in *Figure 7* is visualized in a B-scan, an alternative viewpoint of the raw data, to stack the raw reflections together. This has the potential to highlight factors that were previously hidden in the time domain data. A B-scan for a 50° CA range centered around the TDC of the Top Ring sensor at 100% loading steady-state operation is shown in *Figure 8*.

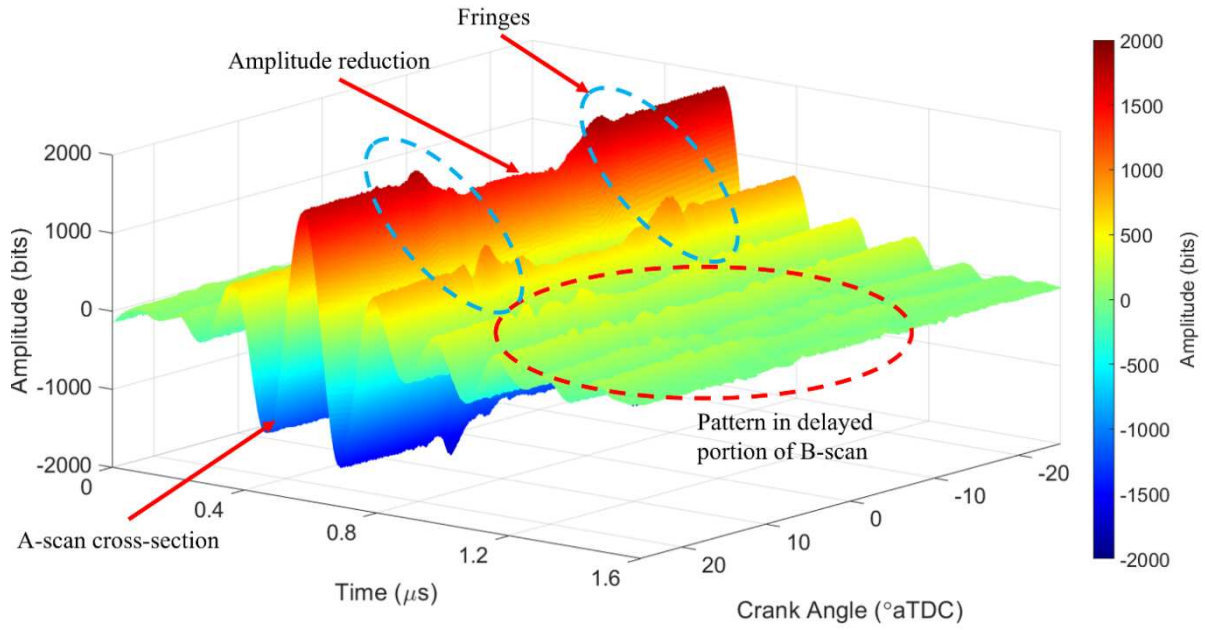

Figure 8 B-scan for the Top Ring sensor.

The predominant visual pattern in *Figure 8* is the decrease in amplitude of the large peaks seen for time 0.4 – 0.8 μs. This section of the recorded data is the driving force of the Frequency Index method (steps d-f in *Figure 6*). Following on from the decayed amplitude of successive peaks (after time 0.8 μs) there is also a pattern between the reflections which was unnoticed in the previous data processing route. This pattern is displayed clearer from a top-down view of the B-scan, see *Figure 9(a)* for the whole recorded reflection in the time domain. The trailing portion of the B-scan is shown in *Figure 9(b)* with a reduced amplitude range to highlight any minor patterns in the results.

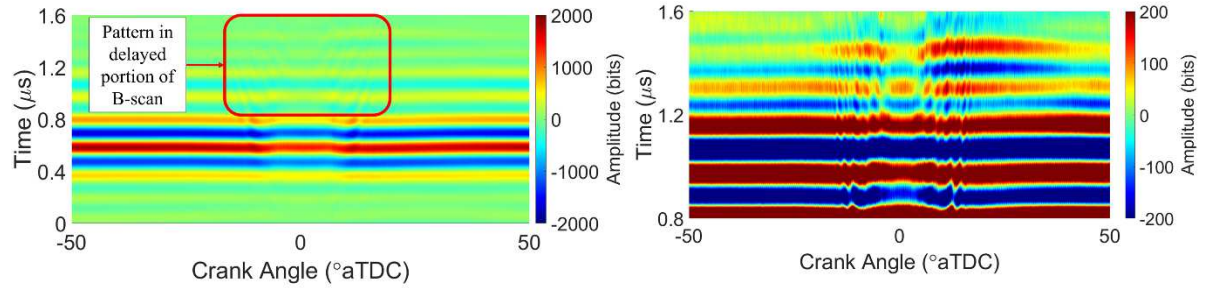

Figure 9 (a) 2D view of the B-scan replotted from the data in *Figure 8*. (b) Trailing edge of *Figure 9(a)*.

The trailing edge of the B-scan displayed in *Figure 9(b)* shows a complex pattern of waves that were previously hidden when analysis studied each time domain reflection individually. This B-scan shows a pattern that extends from -16° to 16° CA. However, geometric analysis on the piston indicated that the top piston ring was aligned with the Top Ring sensor from -8.5° to 8.5° CA. Therefore, a significant portion of this B-scan pattern is outside of the ring alignment zone.

To aid in the visualization of this effect the mean reference reflection has been removed from each reflection ($A(t)$-$A_{ref}(t)$) so that the B-scan shows the change in amplitude from the reference reflection at each data point, this is shown in *Figure 10*.

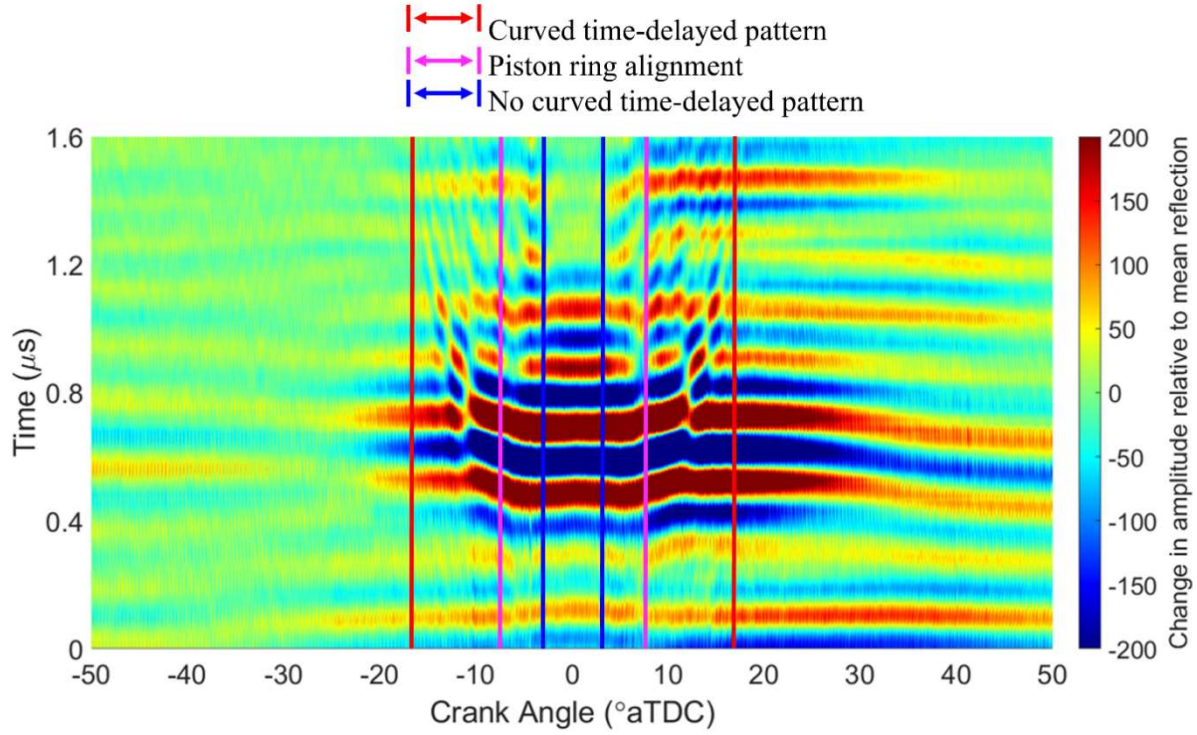

Figure 10 B-scan for the Top Ring sensor having removed the reference reflection.

The time-domain reflection example in *Figure 6(c)* indicated the main body of the reflection used in the previous analysis could typically be defined between time 0.3 and 0.9 μs, represented in *Figure 10* by the large change in amplitude from the reference at these points. In addition to the main body reflection, the true extent of the time-delayed pattern previously hidden in the B-scan is shown.

The prominent pattern is the time-delayed interference which shows a curved constructive and destructive interference pattern that extends from -16° to 16° CA (indicated via the red lines in *Figure 10*). This occurs at a much greater CA range than when the ring is aligned with this transducer (-8.5° to 8.5° CA shown via the pink lines). The curved pattern is not present over the whole range from -16° to 16° CA, as from -3° to 3° CA (blue lines) the time-delayed variation is no longer observed. This is when the piston ring is near full alignment (95% alignment) with the sensor, suggesting that outside of this range it may be unsuitable for OFT calculation using the Frequency Index method, as other factors are impacting the reflection which would have a significant effect on the FFT and thus reflection coefficient/OFT calculation.

The B-scan also shows an alternative visualization of the extensive variation in reflection coefficient post piston ring, seen in *Figure 7*. The change in amplitude from the reference reflection is seen from 16° to 50° CA that is not seen before the ring (-50° to -16° CA). The large CA range of this factor and those of the curved interference (-16° to 16° CA) indicate the likelihood of adjacent piston rings impacting the measurement of each other due to their close proximity.

Previous ultrasonic piston ring film thickness analysis is based upon the concept that a reflected wave from the piston ring is only detected when the ring was aligned over the transducer. This is shown to not be the case in *Figure 10* by the time-delayed change in the reflected wave whose time delay decreases as the ring approaches the sensor. The pattern is

symmetric about the TDC and observed over a greater range than piston ring alignment with the sensor. The symmetric nature is theorized to be due to the time delay from the wavefront spreading and reaching a piston ring outside of the alignment zone that is reflected towards the transducer. When the piston ring is further from the sensor the ultrasonic wave is traveling a greater distance to travel back to the transducer, which causes a greater time delay before being recorded. The time delay reduces as the piston ring approaches leading to the curved pattern as seen in *Figure 10*. The pattern is observed until there is no delay when the ring is suitably aligned. Four cases of ultrasonic reflections are theorized from the ring-liner interaction, see *Figure 11* for a visualization of this.

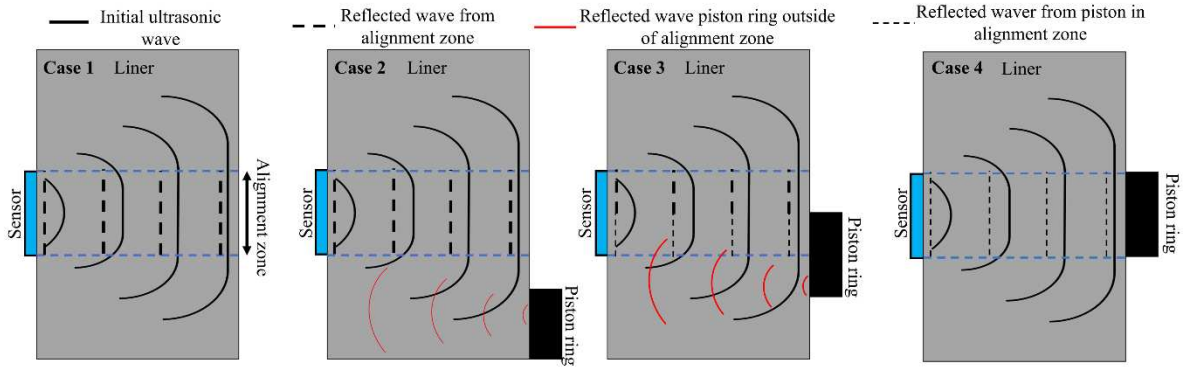

Figure 11 Wave propagation through the liner.

The four cases in *Figure 11* are summarized as follows:

- Case 1: Piston ring not aligned and significantly far away - The only portion of the reflected wave reaching the sensor is from the alignment zone.
- Case 2: Piston ring moves up the liner - The ultrasonic wave outside of the alignment region starts to reflect from the piston ring with a portion being reflected towards the sensor. The reflections from outside the alignment zone are first detected at -16° CA and the time delay reduces as the ring approaches. As the ring is not aligned with the sensor the constructive/destructive interference from the ring causes fluctuations in the reflection coefficient (fringe effects) centered about unity (R=1).
- Case 3: Partial alignment of the piston ring - The partial alignment causes a drop in reflection coefficient however, there are still reflections from outside the alignment zone being recorded. The combination of constructive/destructive interference and partial alignment causes a drop in reflection coefficient that fluctuates, equivalent to -8.5° to -3° CA and 3° to 8.5° CA.
- Case 4: Full ring alignment - A significant drop in reflection coefficient as the ring is fully aligned. No reflections from outside of the alignment zone are directed to the sensor, therefore no time delayed factors are seen, equivalent to -3° to 3° CA.

The four cases outlined in *Figure 11* are overlayed onto the reflection coefficient for the Top Ring sensor at 100% loading steady-state operation from *Figure 7* in *Figure 12*.

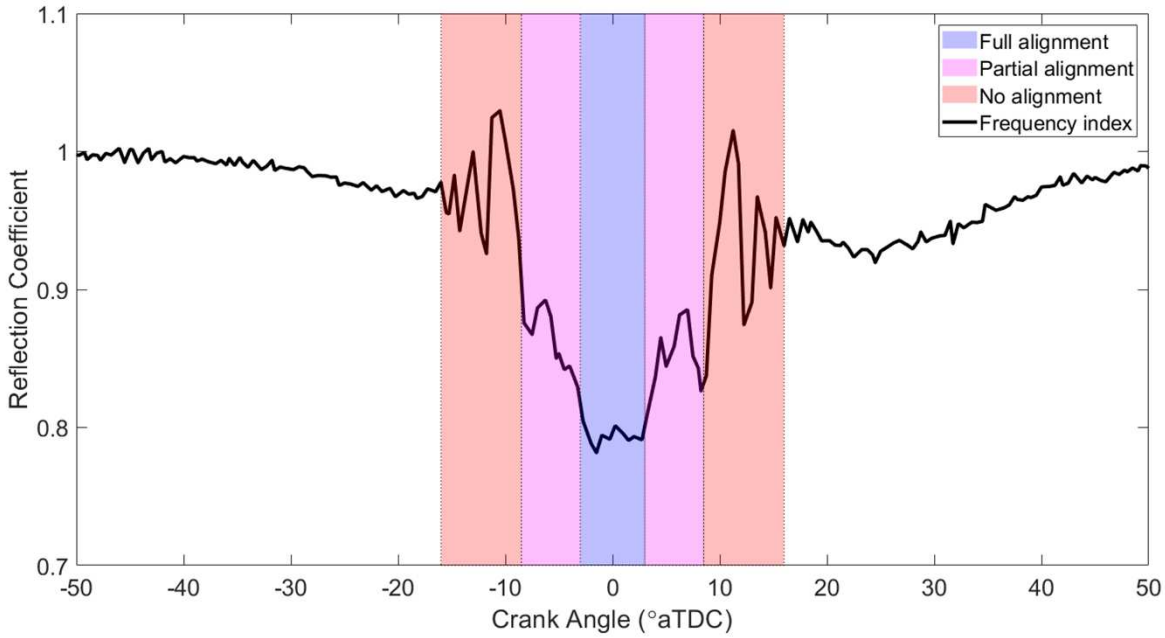

Figure 12 Alignment stages overlayed over the reflection coefficient from the Frequency Index method.

The four cases identified in *Figure 11* provide a near-perfect alignment with the trends seen in the reflection coefficient from the Frequency Index method in *Figure 7*. Indicating that the reflections from outside the alignment zone, visualized in the B-scan, may be causing a number of these trends in the Frequency Index data. The reflection coefficient, therefore, appears to only be unhindered from the constructive/destructive interference from -3° to 3° CA. At ±3° CA, this corresponds to 95% alignment between the piston ring and sensor before the trailing pattern is no longer measurable.

The presence of ultrasonic reflections from outside of the piston ring alignment zone may explain the extent of the fringe effect seen in *Figure 7* as it is typically greater than that seen in ultrasonic piston ring work in automotive engines [11], [29]–[33]. This is primarily thought to be due to the increased path length in marine diesel engines as the liner is significantly thicker, typically over 100 mm in marine diesel engines versus several mm in automotive engines. The order of magnitude greater path length provides a greater distance for the ultrasonic wavefront to spread. Therefore, reflections from when the piston ring is a greater distance from the alignment zone are detected in marine diesel engines than could be detected in automotive engines leading to a greater fringe effect.

5 Control sensor

An additional ultrasonic sensor was instrumented above all piston rings at their TDC positions as in principle, the sensor should experience no discernible change in reflection coefficient with CA as nothing would move into the sensors' alignment region. However, the B-scan in *Figure 10* indicated that this is clearly not the case. The reflection coefficient for this sensor at 100% loading is shown in *Figure 13*.

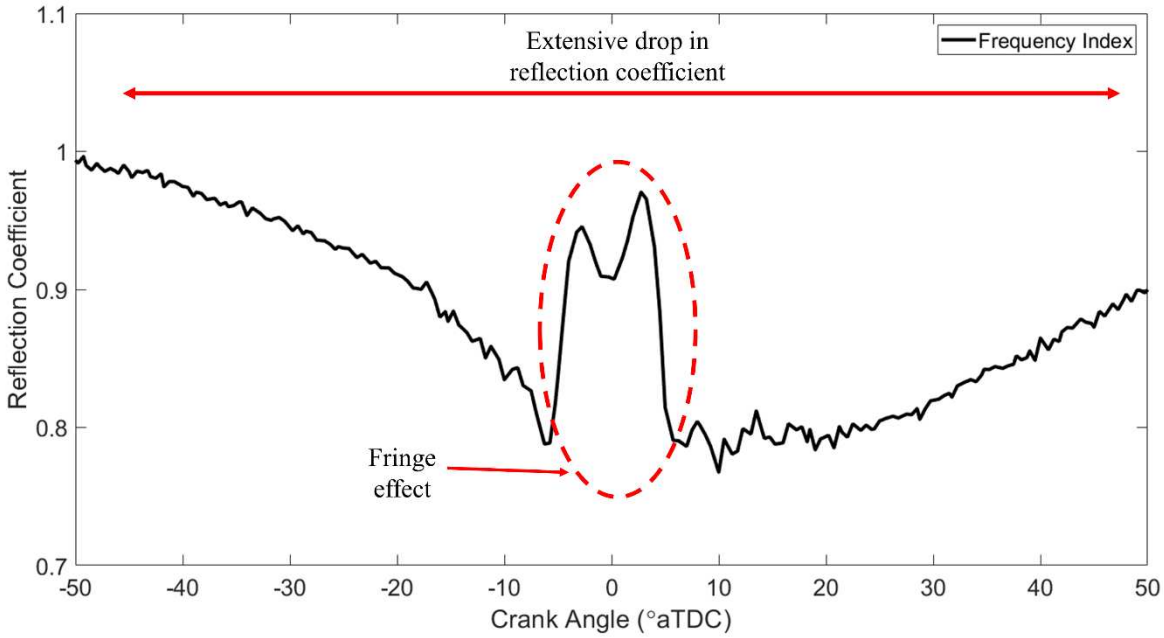

Figure 13 Reflection coefficient over the Control sensor at 100% loading.

Counter-intuitively, *Figure 13* shows that there was a significant change in reflection coefficient over the 100° CA range, with a decrease seen for the majority of the CA range, even with no piston ring aligning with this sensor. Noticeably the trend in variation is very different from those seen for the Top Ring sensor (*Figure 7*) which was aligned with the first ring at the TDC. The presence of this variation without a piston ring further indicates a more complex interaction between a piston ring and sensor is occurring than previously considered. In relation to the four cases theorized, this sensor experiences Case 1 and 2, therefore only the fringe effect is observed. Due to the inflexion of the piston ring marginally beneath this sensor, it causes the fringe effects to join over the TDC for this sensor. The cause of the drop in reflection coefficient over the large CA range is currently unknown. This sensor was instrumented 20 mm above the first piston ring at the TDC (the same distance between adjacent piston rings) therefore, measurements of each piston ring will have been subject to reflections from adjacent piston rings. In the case of the Top Ring sensor (*Figure 7*), the second piston ring will have been detected when the piston was at the TDC.

5.1 k-Wave simulation

To further study the ultrasonic wave theorizations and trends seen for the reflection coefficient from the Control sensor, a simulation was developed. Using k-Wave, an open-source MATLAB toolbox established in [40]–[42].

The developed model consists of pulsing an ultrasonic wave through a medium and recording the reflection from the other side that has a full lubricating film. The simulation is run multiple times (> 750) with each simulation moving the ’piston ring’ across the domain, equivalent to a piston ring moving up the cylinder liner and stopping marginally before piston ring alignment with the sensor, equivalent to that experienced by the Control sensor. In k-Wave, a domain is defined, and the speed of sound and density is set at each node. In the case of a piston ring and cylinder liner example, the model parameters are defined in *Table 2*.

Table 2 k-Wave model parameters.

Model parameter	Value	Unit
Domain size	640x2560 4x20	- mm
Input signal	1	MHz
Liner speed of sound **Liner density**	5000 7300	m/s kg/m^3
Oil speed of sound **Oil density**	1007 781	m/s kg/m^3
Piston ring speed of sound **Piston ring density**	6000 7850	m/s kg/m^3

An example of the domain for two simulations is shown in *Figure 14* in which the upper plots show a simulation with the piston ring significantly far from the sensor, whilst the lower plots are for a near aligned piston ring. The solid media are shown in black, whilst the liquid (engine oil) is shown in white. A zoomed-in version of the lower speed of sound plot shows the thin lubricating layer between the piston ring and liner.

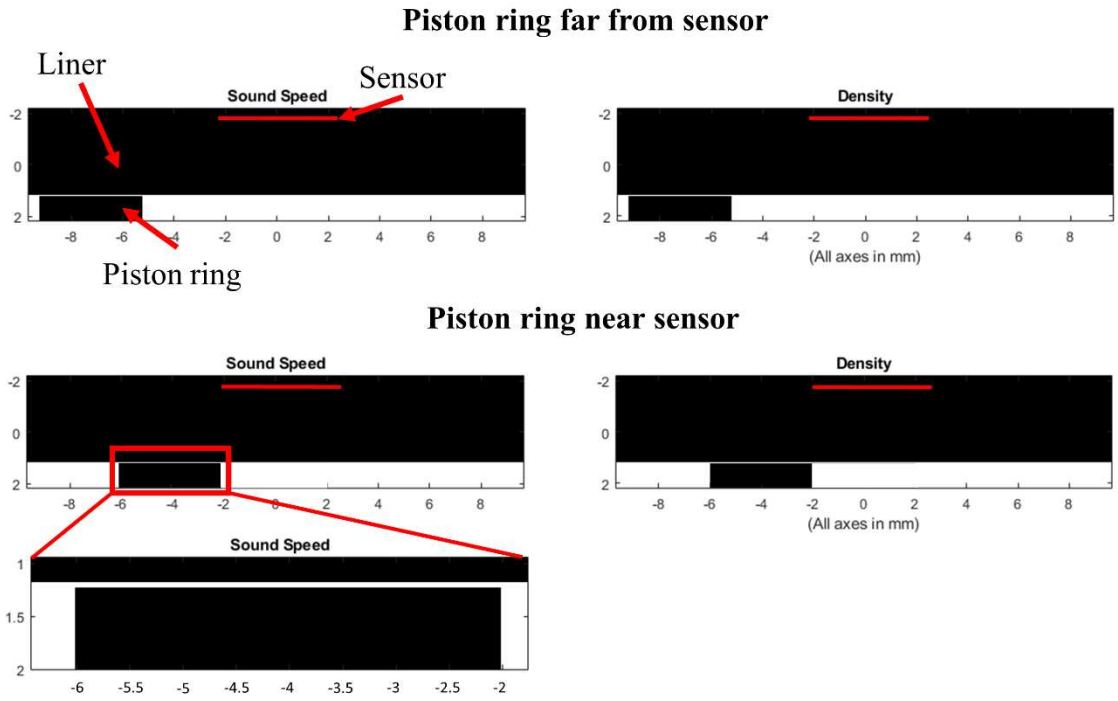

Figure 14 k-Wave domain for two simulation examples.

The series of simulations produced an ultrasonic reflection from each piston ring position. By processing these reflections using the method shown in *Figure 6(c)-(e)*, to produce an FFT and defining the reflection coefficient at 1 MHz, the reflection coefficient for the simulation is produced as shown in *Figure 15*.

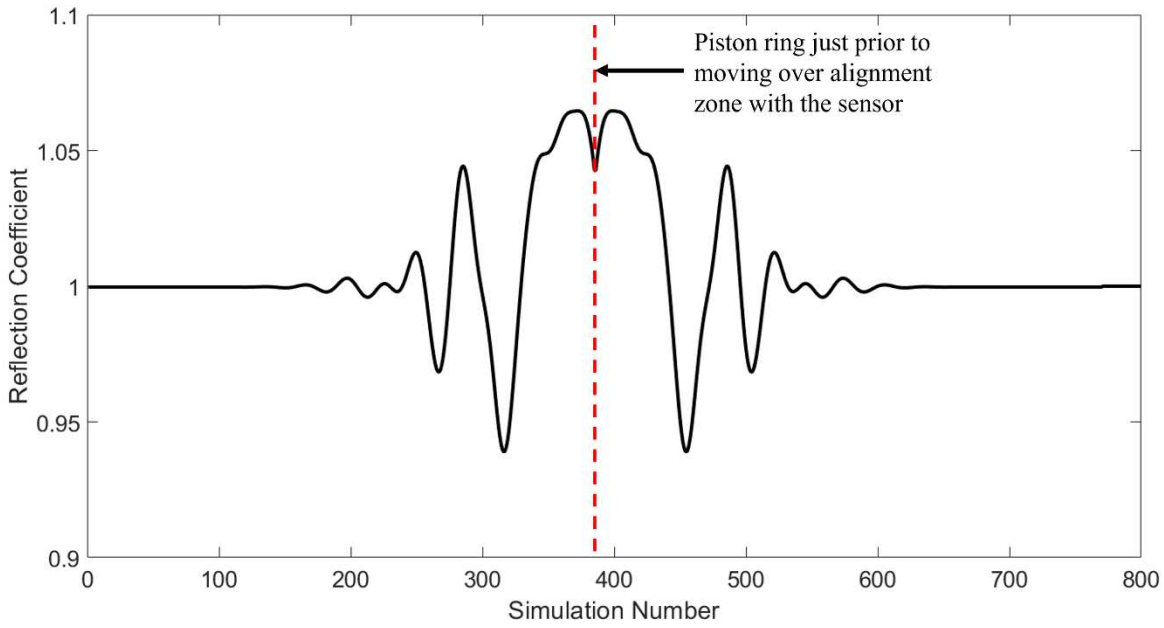

Figure 15 Reflection coefficient simulation for the Control sensor.

The sharp rise and dip in reflection coefficient immediately before and after the TDC (Simulation 385) in *Figure 15* is similar to that previously shown in the experimental results in *Figure 13*. Further indicating that the approaching piston ring combined with the spreading of the ultrasonic wavefront leads to additional energy to be reflected towards the sensor. The magnitude of the fringe effect is proportional to the CA range in which a piston ring is in proximity to the sensor, therefore the impact is reduced on rings further down the liner as the piston had a greater velocity here.

Notably, there is no reduction in the reflection coefficient over an extended CA range in the simulation. There are several potential causes for this:

- The model is entirely based on wave propagation, therefore it does not consider engine factors impacting the sensor, such as the impact of cylinder pressure or combustion products.
- Potential error in transducer instrumentation placement leading to the experimental transducer experiencing unanticipated reflections.
- The liner is assumed to be an anisotropic elastic solid which is not the case in cast iron.
- The model used a "perfect" 1 MHz input and assumes the ring is a constant distance from the liner of 12 μm. Both of these differ from the experimental results due to noise in the system and the piston rings relative freedom to vary the distance from the liner surface.

6 Hilbert Envelope method

The reflection coefficient used hitherto was defined using the Frequency Index method by indexing the FFT at the transducer central frequency and has been used in piston ring work such as [10], [11], [29]–[33]. In the case of the RTX-6, the method has the disadvantage that it is subject to reflections from outside the piston ring alignment zone as extensively shown via the B-scans, Control sensor, and the k-Wave simulation. The FFT used for the Frequency

Index method produces a measure of energy distribution at different frequencies, therefore, ensuring that only the desired reflection is used to produce the FFT is of key importance but potentially difficult to define in practice. An alternative route is to use the 'Hilbert Envelope' method, by using the peak of the Hilbert envelope to define the reflection coefficient. The Hilbert envelope is shown in blue in *Figure 6(c)* and tracking the peak of the envelope ensures that only the time instant of the maximum amplitude of the reflection is considered (for example, the peak is at time 0.65 μs in *Figure 10*), therefore time-delayed reflections inside and outside of the piston ring alignment region have no impact on the Hilbert Envelope method reflection coefficient.

The reflection coefficient from the Frequency Index and Hilbert Envelope methods at 100% loading at steady-state operation are shown in *Figure 16*.

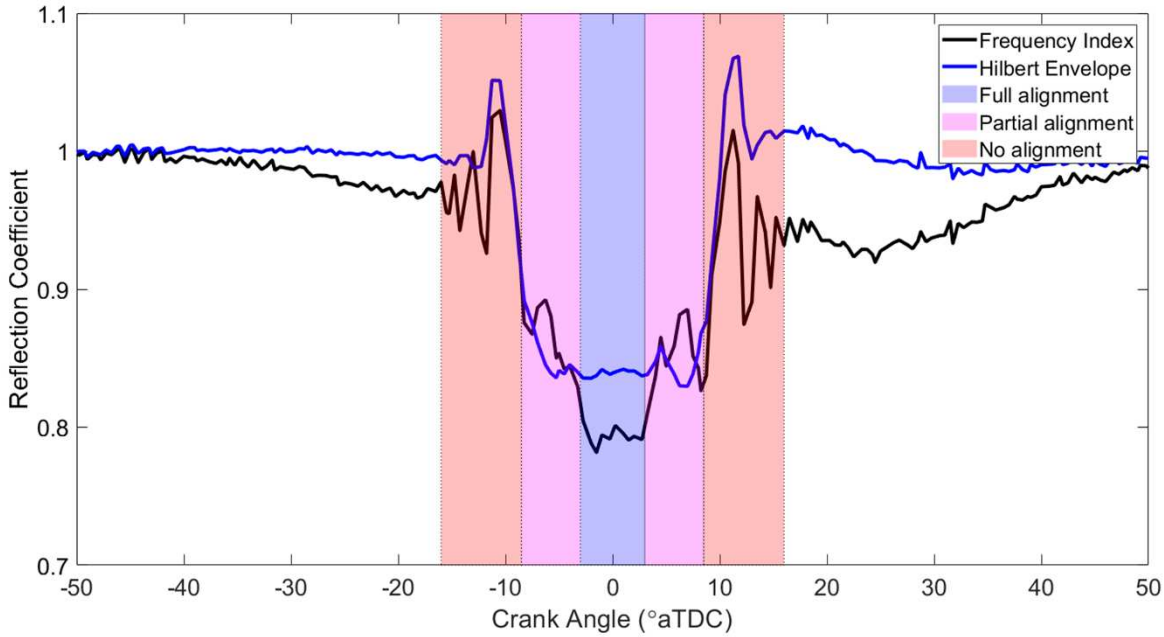

Figure 16 Reflection coefficient for the Top Ring sensor from the Frequency Index and Hilbert Envelope methods.

In *Figure* 7 a series of secondary features in the Frequency Index data were identified both within and outside of the alignment zone of the first piston ring. A comparison of the Frequency Index method to the Hilbert Envelope method in *Figure 16* displays that the Hilbert Envelope is not exposed to a number of these. Thus, indicating that those secondary features are found in the Frequency Index results are merely due to the data processing method as opposed to a factor from the marine engine itself. The Hilbert Envelope reduces the presence of a prolonged change in reflection coefficient before/after the ring pack. Leading to a less unusual result, that the reflection coefficient remains at unity when there is no piston ring over the transducer. The fringe effects immediately before and after the ring pack is also reduced by the Hilbert Envelope to a single peak. The secondary fringe in the alignment zone that has been seen in numerous ultrasound research of varying applications ([10], [30], [38], [39]) is also minimized and nearly completely removed from the application of the Hilbert Envelope.

The key variation between the two methods is the timespan they consider, as the Frequency Index provides a summary of the summation of the whole reflection from the piston ring plus

to some extent, the response from other microvariations and noise in the system due to difficulties identifying the start and end of the reflection. Whilst the Hilbert Envelope only covers the maximum amplitude portion of the reflection (the reflection from the piston ring). This, therefore, indicates that the factors that lead to; prolonged reflection coefficient variation, fringe effects, and the multiple dips in the alignment zone are not from the peak of the reflection but factors that arise from the summation of frequencies over a greater time span, as was also seen in the B-scans and for the Control sensor.

Similar trends are seen in the comparison between the Frequency Index and Hilbert Envelope reflection coefficient for the Control sensor in *Figure 17*.

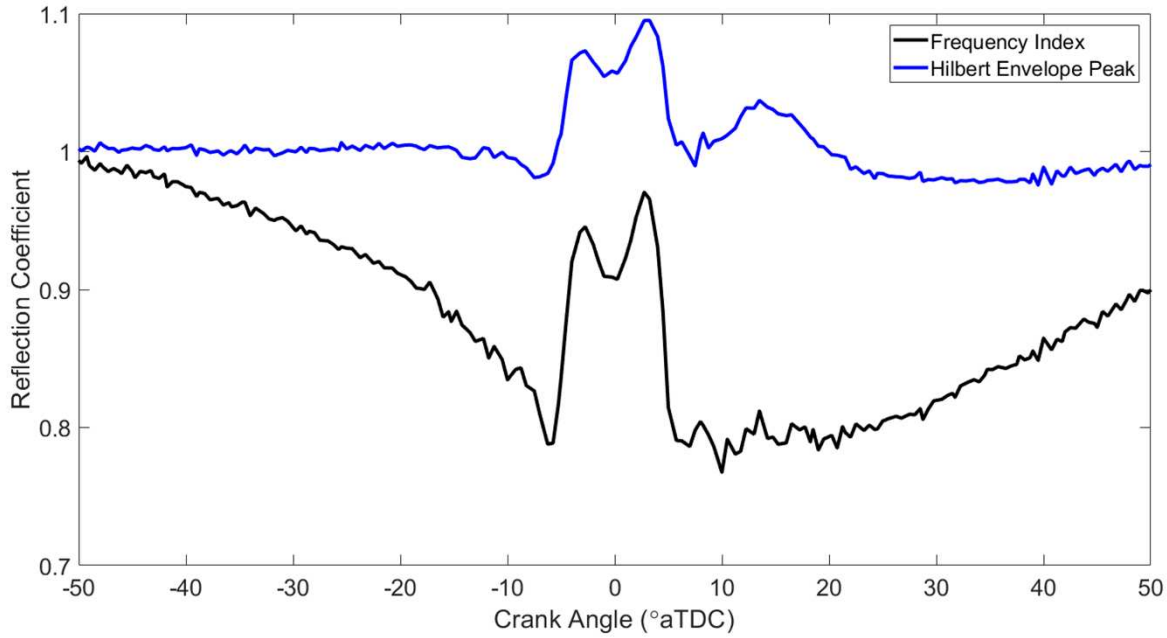

Figure 17 The reflection coefficient from the Frequency Index and Hilbert Envelope method for the Control sensor at 100% loading.

The true extent of the difference in the data processing methods is visible in *Figure 17*. The excessive reduction in reflection coefficient over the 100° CA range shown is completely removed via the Hilbert Envelope. This method reveals a small peak at 13° CA, shortly after the maximum combustion pressure.

The fringe effect itself is present in both methods from -6° to 6° CA but to a reduced extent in the Hilbert Envelope (0.1 increase using the Hilbert Envelope, versus 0.2 for the Frequency Index). Overall, for the Control sensor, the Hilbert Envelope removes the unexplainable drop in reflection coefficient leading to the reflection coefficient being more similar to the k-Wave simulation in *Figure 15*.

6.1 Oil film thickness

The reflection coefficient for the two data processing techniques has been converted into OFT using Equation 5 as shown in *Figure 18*. This is only presented for the Top Ring sensor as the Spring Model is only applicable for an oil film confined by two solid bodies, therefore it is not applicable for the Control sensor.

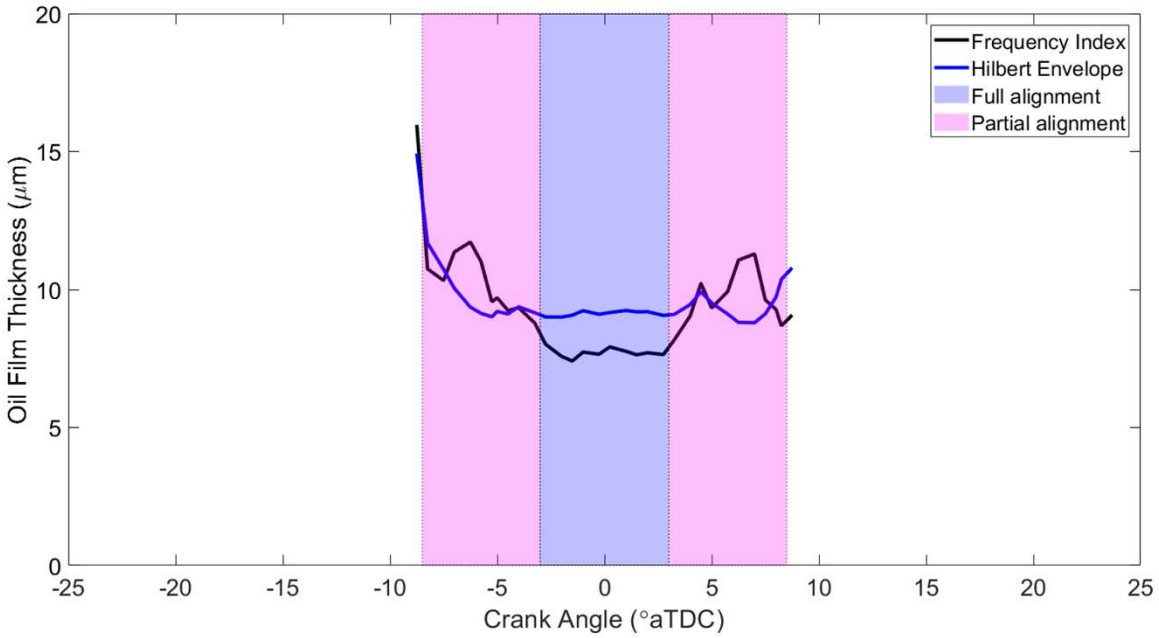

Figure 18 Oil film thickness from the Top Ring sensor using the Frequency Index and Hilbert Envelope methods at 100% loading steady-state operation.

The OFT from the two methods provide oil films in the low micron order of magnitude. The Frequency Index ranges from 7-10 μm whereas the Hilbert Envelope ranges from 8-13 μm. The Hilbert Envelope indicates a consistently thicker oil film, roughly 20% close to the TDC, and a more consistent value across the alignment region of the first piston ring. The OFT is largely level from -6.5° to 4° CA. The Frequency Index OFT is only greater at two distinct points, ±6.5° CA when the secondary fringe effect from partial ring alignment was seen in the reflection coefficient from this method.

6.2 Minimum oil film thickness

The minimum OFT (MOFT) from the Frequency Index and Hilbert Envelope methods has been isolated from each data capture at the three loading steps considered for the Top Ring sensor. This data is presented in *Figure 19* for 100% loading, steady-state engine operation. The mean MOFT across steady-state engine operation and the coefficient of variance (COV) at all loading steps for both processing methods are presented in *Table 3*.

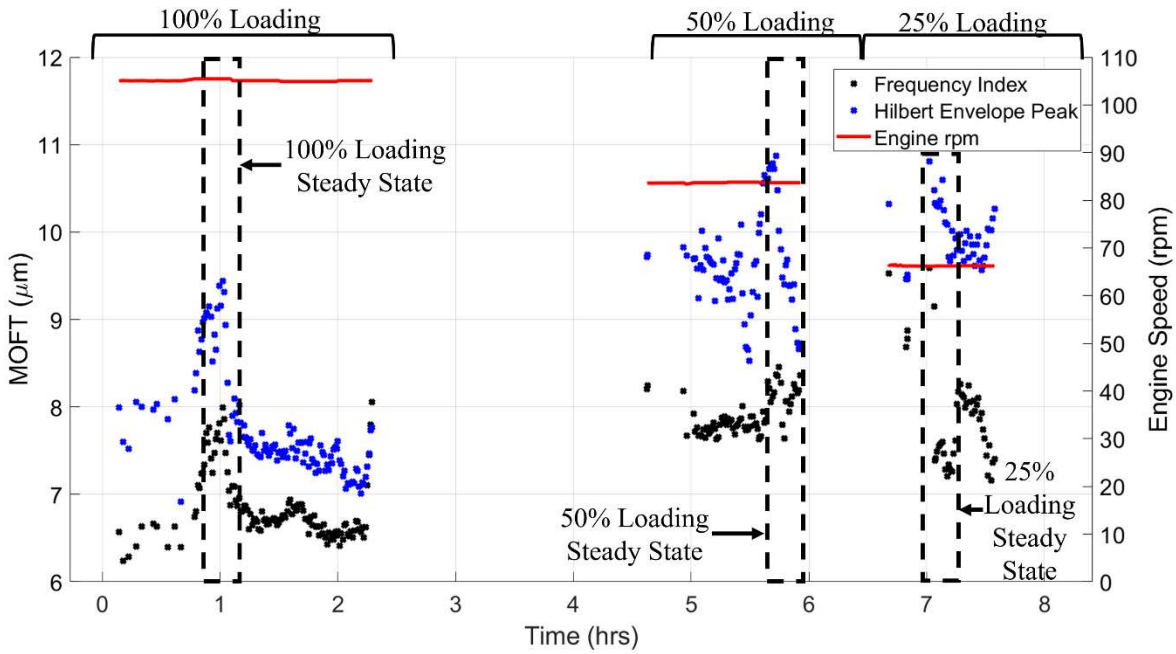

Figure 19 MOFT from the Frequency Index and Hilbert Envelope methods at all loading levels.

Table 3 Steady-state MOFT across all loading levels from the Frequency index and Hilbert Envelope methods.

Engine loading (%)	Frequency Index		Hilbert Envelope	
	MOFT (µm)	COV (%)	MOFT (µm)	COV (%)
100	7.4	4.6	8.9	3.7
50	8.1	2.4	9.8	7.5
25	7.9	10.4	10.4	1.9

Both data analysis methods presented in *Figure 19* show the same overall trends in MOFT, as the engine loading is decreased the MOFT increased. This is expected as under lower engine loading the combustion pressure is reduced leading to lower conformity between the piston ring and liner, therefore providing thicker lubricating films. Although the MOFT ranges are different for each method; the Frequency Index approach ranged from 6.2-9.1 mm whilst the Hilbert Envelope ranges from 7.0-11.0 mm. This represents a typical increase in the MOFT of 20% for the Hilbert Envelope method which is visible for most data captures both within and outside of steady-state testing.

From observation of purely the steady-state engine loading periods, the same trend of MOFT is shown in the averaged steady-state data presented in *Table 3*. However, the COV over this steady-state period is affected by the data processing technique. The Frequency Index method has a greater average and peak COV value indicating a greater consistency between captures is shown from the Hilbert Envelope method.

7 Conclusions

Ultrasonic sensors have been instrumented onto an RTX-6 test engine, a Winterthur Gas & Diesel marine diesel engine to study the piston ring oil film thickness at the top dead center. The main findings can be summarized as follows:

- In previous works, a Frequency Index of the fast Fourier transform was commonly used to define the reflection coefficient. An inspection of B-scans and a Control sensor above all piston rings at their top dead center positions in combination with a k-Wave model has shown significant detection of the piston ring outside of the anticipated alignment zone. This was therefore affecting the reflection coefficient values when using the Frequency Index method.
- The impact of the time-delayed ultrasonic reflections has been reduced by using the peak of the Hilbert envelope to define the reflection coefficient. Thus, removing several trends seen in previous ultrasonic piston ring works.
- The oil film thickness from the two processing methods has been evaluated, showing the minimum oil film thickness to typically be 20% greater for the Hilbert Envelope method. Indicating the Frequency Index method, which was subject to the undesired reflections was providing an underestimation of the true film thickness.
- Across the load range considered the Hilbert Envelope method showed the minimum oil film thickness to vary with load, at full load the film minimum was 8.9 μm ranging up to 10.4 μm at 25% loading.

Acknowledgements

The authors would like to acknowledge the financial support from three sources; the EU framework program for research and innovation Horizon 2020 Grant Agreement No:634135-Hercules-2. The Engineering and Physical Sciences Research Council for RDJ's fellowship on Tribo-Acoustic Sensors EP/ N016483/1; and the EPSRC Centre for Doctoral Training in Integrated Tribology EP/L01629X/1. The authors would also like to thank Winterthur Gas & Diesel and Peak to Peak Ltd for enabling the opportunity to test upon the engine and access to equipment and researcher time. A final thanks to Bradley Treeby, Ben Cox and Jiri Jaros for the development of the open-source k-Wave toolbox.

References

[1] International Maritime Organization, "Resolution MEPC.304(72) - Initial IMO Strategy on Reduction of GHG Emissions from Ships and Existing IMO Activity Related to Reducing GHG Emissions in the Shipping Sector," 2018.

[2] S. C. Tung and M. L. McMillan, "Automotive Tribology Overview of Current Advances and Challenges for the Future," *Tribol. Int.*, vol. 37, no. 7, pp. 517–536, 2004, doi: 10.1016/j.triboint.2004.01.013.

[3] D. E. Richardson, "Review of Power Cylinder Friction for Diesel Engines," *J. Eng. Gas Turbines Power*, vol. 122, no. 4, pp. 506–519, Oct. 2000, doi: 10.1115/1.1290592.

[4] P. Nagar and S. Miers, "Friction between Piston and Cylinder of an IC Engine: a Review," *SAE Tech. Pap. 2011-01-14*, 2011, doi: 10.4271/2011-01-1405.

[5] J. Beulshausen, S. Pischinger, and M. Nijs, "Drivetrain Energy Distribution and Losses from Fuel to Wheel," *SAE Int. J. Passeng. Cars - Mech. Syst.*, vol. 6, no. 3, pp. 1528–

1537, 2013, doi: 10.4271/2013-01-9118.

[6] K. Froelund and E. Yilmaz, “Impact of Engine Oil Consumption on Particulate Emissions,” 2004.

[7] K. Froelund, S. Fritz, and B. Smith, “Lubricating Oil Consumption Measurements on An EMD 16-645E Locomotive Diesel Engine,” in *Proceedings of the ASME 2003 Internal Combustion Engine Division Spring Technical Conference. Design, Application, Performance and Emissions of Modern Internal Combustion Engine Systems and Components*, 2003, pp. 361–368, doi: 10.1115/ICES2003-0549.

[8] S. Brynolf, E. Fridell, and K. Andersson, “Environmental Assessment of Marine Fuels: Liquefied Natural Gas, Liquefied Biogas, Methanol and Bio-Methanol,” *J. Clean. Prod.*, vol. 74, pp. 86–95, 2014, doi: 10.1016/j.jclepro.2014.03.052.

[9] G. Belgiorno, G. Di Blasio, and C. Beatrice, “Advances of the Natural Gas/Diesel RCCI Concept Application for Light-Duty Engines: Comprehensive Analysis of the Influence of the Design and Calibration Parameters on Performance and Emissions,” in *Natural Gas Engines. Energy, Environment, and Sustainability*, Singapore: Springer, 2019.

[10] J. Rooke, X. Li, H. Brunskill, M. Stark, and R. Dwyer-Joyce, “Comparison of Ring-Liner Oil Film Thickness Resulting from Different Injector Designs in a Diesel Marine Engine Using an Ultrasound Measurement Method,” *SAE Int. J. Engines*, vol. 14, no. 6, 2021, doi: 10.4271/03-14-06-0053.

[11] R. Mills, E. Y. Avan, and R. S. Dwyer-Joyce, “Measuring Lubricant Films at the Piston-Cylinder Contact: An Overview of Current Technologies with Focus on Ultrasound,” *SAE Tech. Pap. 2013-01-0294*, 2013, doi: 10.4271/2013-01-0294.

[12] M. Takiguchi, R. Sasaki, and I. Takahashi, “Oil Film Thickness Measurement and Analysis of a Three Ring Pack in an Operating Diesel Engine,” *SAE Tech. Pap. 2000-01-1787*, 2000.

[13] A. Dhar, A. K. Agarwal, and V. Saxen, “Measurement of Lubricating Oil Film Thickness Between Piston Ring-Liner Interface in an Engine Simulator,” *SAE Tech. Pap. 2008-28-0071*, pp. 494–499, 2008.

[14] A. Dhar, A. K. Agarwal, and V. Saxena, “Measurement of Dynamic Lubricating Oil Film Thickness Between Piston Ring and Liner in a Motored Engine,” *Sensors Actuators, A Phys.*, vol. 149, no. 1, pp. 7–15, 2009, doi: 10.1016/j.sna.2008.09.021.

[15] G. Garcia-Atance Fatjo, E. H. Smith, and I. Sherington, “Mapping Lubricating Film Thickness, Film Extent and Ring Twist for the Compression-Ring in a Firing Internal Combustion Engine,” *Tribology International*, vol. 70. pp. 112–118, 2014, doi: 10.1016/j.triboint.2013.10.001.

[16] G. Garcia-Atance Fatjo, E. H. Smith, and I. Sherrington, “Piston-ring film thickness: Theory and experiment compared,” *Proc. Inst. Mech. Eng. Part J J. Eng. Tribol.*, vol. 232, no. 5, pp. 550–567, 2018, doi: 10.1177/1350650117722257.

[17] S. J. Söchting and I. Sherrington, “The Effect of Load and Viscosity on the Minimum Operating Oil Film Thickness of Piston-Rings in Internal Combustion Engines,” *Proc. Inst. Mech. Eng. Part J J. Eng. Tribol.*, vol. 223, no. 3, pp. 383–391, 2009, doi: 10.1243/13506501JET556.

[18] D. O. Ducu, R. J. Donahue, and J. B. Ghandhi, “Design of Capacitance Probes for Oil Film Thickness Measurements Between the Piston Ring and Liner in Internal Combustion,” *J. Eng. Gas Turbines Power*, vol. 123, pp. 633–643, 2001, doi: 10.1115/1.1368116.

[19] M. Takiguchi, K. Nakayama, S. Furuhama, and H. Yoshida, “Variation of Piston Ring Oil Film Thickness in an Internal Combustion Engine - Comparison Between Thrust and Anti-Thrust Sides,” *SAE Tech. Pap. 980563*, 1998, doi: 10.4271/980563.

[20] T. Seki, K. Nakayama, T. Yamada, A. Yoshida, and M. Takiguchi, “A Study on Variation in Oil Film Thickness of a Piston Ring Package: Variation of Oil Film Thickness in Piston Sliding Direction,” *JSAE Rev.*, vol. 21, no. 3, pp. 315–320, 2000, doi: 10.1016/S0389-4304(00)00044-8.

[21] R. S. Notay, M. Priest, and M. F. Fox, “The Influence of Lubricant Degradation on Measured Piston Ring Film Thickness in a Fired Gasoline Reciprocating Engine,” *Tribol. Int.*, vol. 129, no. January 2019, pp. 112–123, 2019, doi: 10.1016/j.triboint.2018.07.002.

[22] Y. Baba, H. Suzuki, Y. Sakai, D. L. T. Wei, T. Ishima, and T. Obokata, “PIV/LIF Measurements of Oil Film Behavior on the Piston in I.C. Engine,” *SAE Tech. Pap. 2007-24-0001*, 2007, doi: 10.4271/2007-24-0001.

[23] L. L. Ting, “Development of a Laser Fluorescence Technique For Measuring Piston Ring Oil Film Thickness,” *J. Lubr. Technol.*, vol. 102, no. 2, pp. 165–170, 1980, doi: 10.1115/1.3251458.

[24] R. Taylor and P. Evans, “In-situ Piston Measurements,” *Proc. Inst. Mech. Eng. Part J J. Eng. Tribol.*, vol. 218, no. 3, pp. 185–200, 2004.

[25] J. Tamminen, C. Sandström, and P. Andersson, “Influence of Load on the Tribological Conditions in Piston Ring and Cylinder Liner Contacts in a Medium-Speed Diesel Engine,” *Tribol. Int.*, vol. 39, no. 12, pp. 1643–1652, 2006, doi: 10.1016/j.triboint.2006.04.003.

[26] T. A. Dow, C. A. Schiele, and R. D. Stockwell, “Technique for Experimental Evaluation of Piston Ring- Cylinder Film Thickness,” *J. Lubr. Technol.*, vol. 105, no. 3, pp. 353–360, 1983, doi: https://doi.org/10.1115/1.3254608.

[27] P. Saad, L. Kamo, M. Mekari, W. Bryzik, V. Wong, N. Dmytrychenko, and R. Mnatsakanov, “Modeling and Measurement of Tribological Parameters Between Piston Rings-Liner in Turbocharged Diesel Engine,” *SAE Tech. Pap. 2007-01-1440*, 2007, doi: 10.1115/IJTC2006-12308.

[28] M. A. Bulsara, D. V. Bhatt, and K. N. Mistry, “Measurement of Oil Film Thickness Between Piston Ring and Liner using Strain Gauge,” *Ind. Lubr. Tribol.*, vol. 65, no. 5, pp. 297–304, 2013, doi: 10.1108/ILT-02-2011-0013.

[29] E. Y. Avan, R. Mills, and R. S. Dwyer-Joyce, “Ultrasonic Imaging of the Piston Ring Oil Film During Operation in a Motored Engine - Towards Oil Film Thickness Measurement,” *SAE Int. J. Fuels Lubr.*, vol. 3, pp. 786–793, 2010, doi: 10.4271/2010-01-2179.

[30] R. Mills, “Ultrasonic measurement of lubricant films generated at the piston-cylinder interface of internal combustion engines,” University of Sheffield, 2012.

[31] R. Mills, J. Vail, and R. Dwyer-Joyce, “Ultrasound for the Non-Invasive Measurement of Internal Combustion Engine Piston Ring Oil Films,” *Proc. Inst. Mech. Eng. Part J J. Eng. Tribol.*, vol. 229, no. 2, pp. 207–215, 2015, doi: 10.1177/1350650114552538.

[32] R. S. Mills, E. Y. Avan, and R. S. Dwyer-Joyce, “Piezoelectric Sensors to Monitor Lubricant Film Thickness at Piston–Cylinder Contacts in a Fired Engine,” *Proc. Inst. Mech. Eng. Part J J. Eng. Tribol.*, vol. 227, no. 2, pp. 100–111, 2012, doi: 10.1177/135065011246483.

[33] R. Mills and R. Dwyer-Joyce, “Ultrasound for the Non-Invasive Measurement of IC Engine Piston Skirt Lubricant Films,” *Proc. Inst. Mech. Eng. Part J J. Eng. Tribol.*, vol. 228, no. 11, pp. 1330–1340, 2014, doi: 10.1177/1350650114538616.

[34] R. S. Dwyer-Joyce, D. A. Green, P. Harper, R. Lewis, S. Balakrishnan, P. D. King, H. Rahnejat, and S. Howell-Smith, “The Measurement of Liner - Piston Skirt Oil Film Thickness by an Ultrasonic Means,” *SAE Tech. Pap. 2006-01-0648*, 2006, doi: 10.4271/2006-01-0648.

[35] M. Stark and R. Mittler, “Optimization of Tribodynamic Effects to Improve the Reduction Potential of Particulate Matter Concentrations in the Exhaust Gas of Large Two Stroke Marine Diesel Engines,” *SAE Int. J. Fuels Lubr.*, vol. 7, no. 3, pp. 965–978, 2014, doi: 10.4271/2014-01-2844.

[36] M. Schoenberg, “Elastic Wave Behavior Across Linear Slip Interfaces,” *J. Acoust. Soc. Am.*, vol. 68, no. 2, pp. 1516–1521, 1980.

[37] R. S. Dwyer-Joyce, B. W. Drinkwater, and C. J. Donohoe, “The measurement of lubricant-film thickness using ultrasound,” *R. Soc.*, no. 459, pp. 957–976, 2003.

[38] A. Hunter, “Ultrasonic Measurements of the Strip Thickness, Lubricant Film Thickness, Roll Deflection and Roll Stress in the Roll Bite in the Cold Rolling of Steel,” University of Sheffield, 2018.

[39] T. Howard, “Development of a Novel Bearing Concept for Improved Wind Turbine Gearbox Reliability,” University of Sheffield, 2016.

[40] B. Treeby and B. T. Cox, “k-Wave: MATLAB toolbox for the simulation and reconstruction of photoacoustic wave fields,” *J. Biomed. Opt.*, vol. 15, p. 21314, 2010, doi: 10.1117/1.3360308.

[41] B. E. Treeby, J. Jaros, D. Rohrbach, and B. T. Cox, “Modelling Elastic Wave Propagation using the k-Wave MATLAB Toolbox,” *IEEE Int. Ultrason. Symp. IUS*, no. 4, pp. 146–149, 2014, doi: 10.1109/ULTSYM.2014.0037.

[42] B. Treeby, B. Cox, and J. Jaros, “k-Wave A MATLAB Toolbox for the Time-Domain Simulation of Acoustic Wave Fields,” 2021. http://www.k-wave.org/ (accessed May 21, 2021).

Abbreviations

CA	Crank Angle
COV	Coefficient of Variance
FFT	Fast Fourier Transform

LIF	Laser Induced Fluorescence
MOFT	Minimum Oil Film Thickness
OFT	Oil Film Thickness
TDC	Top Dead Center
UPR	Ultrasonic Pulser Receiver